J Appl Electrochem (2011) 41:223–233
DOI 10.1007/s10800-010-0227-2

ORIGINAL PAPER

3,4-Dimethoxybenzaldehydethiosemicarbazone as corrosion inhibitor for aged 18 Ni 250 grade maraging steel in 0.5 M sulfuric acid

T. Poornima · Jagannath Nayak · A. Nityananda Shetty

Received: 28 January 2010 / Accepted: 25 September 2010 / Published online: 15 October 2010

Abstract The corrosion inhibition of the aged 18 Ni 250 grade maraging steel in 0.5 M sulfuric acid by 3,4-dimethoxybenzaldehydethiosemicarbazone(DMBTSC) has been investigated by potentiodynamic polarization and electrochemical impedance spectroscopy(EIS) techniques. The inhibition efficiency increased with the increase in inhibitor concentration and decreased with the increase in temperature. Polarization curves indicated mixed type inhibition behavior affecting both cathodic and anodic corrosion currents. The thermodynamic parameters of corrosion and adsorption processes were evaluated. The adsorption of DMBTSC on the aged maraging steel surface was found to obey the Langmuir adsorption isotherm model, and the calculated Gibb's free energy values confirm the spontaneous adsorption. The results obtained by the two techniques were in good agreement.

Keywords Inhibition · Maraging steel · Adsorption · Cathodic reaction · Polarization resistance

T. Poornima
Department of Science and Humanities, PESIT, Bangalore 560085, India

J. Nayak
Department of Metallurgical and Materials Engineering, National Institute of Technology Karnataka, Surathkal, Srinivasnagar, Mangalore, Karnataka 575025, India

A. Nityananda Shetty (✉)
Department of Chemistry, National Institute of Technology Karnataka, Surathkal, Srinivasnagar, Mangalore, Karnataka 575025, India
e-mail: nityashreya@gmail.com

1 Introduction

Corrosion of structural elements is a major issue for any industry because of the chemical environment of chemical processing. Inhibition is one of the most important methods in corrosion protection. Inhibitors protect the metal by adsorbing onto the surface and retard metal corrosion in aggressive environments. Selecting the appropriate inhibitor for specific environment and metal is of great importance, since the inhibitor which protects one particular metal may accelerate the corrosion of another. Maraging steels are special class of ultra high strength steels that differ from conventional steels in that they are hardened by a metallurgical reaction that does not involve carbon [1]. They derive high strength from age hardening of low carbon, Fe–Ni martensitic matrix [2]. The needs of highly reliable substances of high strength and high ductility have gradually increased with the development of aerospace industry. The characteristics of this gray and white steel are high ductility, formability, high corrosion resistance, high temperature strength, ease of fabrication, weldability, and maintenance of an invariable size even after heat treatment [3]. According to the available literature, atmospheric exposure of 18 Ni maraging steel leads to their being corroded in a uniform manner and becoming completely rust covered [4]. Pit depths tend to be shallower than high strength steels [5]. Bellanger and Rameau [6] have studied the effect of slightly acidic pH with or without chloride in radioactive water on the corrosion of maraging steel, and reported that corrosion behavior of maraging steel at the corrosion potential depended on pH, and intermediated remaining on maraging steel surface in the active region favoring the passivity. The effect of carbonate ions in slightly alkaline medium on the corrosion of maraging steel was determined by Bellanger [7]. Heat treatment affects

corrosion rate. Critical and passive current densities increase as the structure is varied from one of being fully annealed to one of fully aged [8]. Maraging steels are found to be less susceptible to hydrogen embrittlement than high-strength steels owing to significantly low diffusion of hydrogen in them [9]. Several technical articles covering alloy design, material processing, thermo-mechanical treatments, welding, strengthening mechanisms, etc., have been published [10]. The maraging steels have emerged as alternative materials to conventionally used quenched and tempered steels for advanced technologies such as aerospace, nuclear, and gas turbine applications. They frequently come into contact with acids during cleaning, pickling, descaling, acidizing, etc. Materials used in acidic environment should have good corrosion resistance.

Thiosemicarbazones and their derivatives have continued to be subjects of extensive investigation in chemistry and biology owing to their broad spectrum of anti-tumor [11, 12], antimalarial [13], and many other applications including corrosion inhibition of metals [14–16]. These compounds can be adsorbed on metal surface through lone pairs of electrons present on nitrogen or sulphur atoms but also through pi electrons present in these molecules [17–20]. Search in the existing literature reveals a very insignificant amount of studies reporting on the corrosion behavior and on the use of inhibitors in controlling corrosion of maraging steel. This study aimed to study the corrosion inhibition of aged 18 Ni 250 grade maraging steel in 0.5 M sulfuric acid medium using DMBTSC as inhibitor.

2 Experimental methods

2.1 Materials

The maraging steel samples (M 250 grade) in aged condition were taken from plates. The solution-annealed and air-cooled plates were subjected to aging treatment at 480 ± 5 °C for 3 h and air cooled. Chemical composition of 18 Ni 250 grade aged maraging steel samples is given in Table 1. Cylindrical test coupons were cut from the plate and sealed with epoxy resin in such a way that the area exposed to the medium is 0.503 cm^2. These coupons were polished as per standard metallographic practice—belt grinding followed by polishing on emery papers of 400, 600, 800, 1000, 1200, and 1500 grades, finally on polishing wheel using legated alumina to obtain mirror finish—degreased with acetone, washed with double-distilled water, and dried in hot air blower before immersing in the corrosion medium.

Table 1 Composition of the aged maraging steel specimen

Element	Composition	Element	Composition
C	0.015%	Ti	0.3–0.6%
Ni	17–19%	Al	0.005–0.15%
Mo	4.6–5.2%	Mn	0.1%
Co	7–8.5%	P	0.01%
Si	0.1%	S	0.01%
O	30 ppm	N	30 ppm
H	2.0 ppm	Fe	Balance

The inhibitor 3,4-dimethoxybenzaldehyde thiosemicarbazone (DMBTSC) was synthesized as per the reported procedure in one-step reaction of 3,4-dimethoxybenzaldehyde with thiosemicarbazide [13]. An equimolar mixture of ethanolic solution of 3,4-dimethoxybenzaldehyde and thiosemicarbazide was taken in a round-bottomed flask. The reaction mixture was refluxed on a hot water bath for about less than 3 h. The precipitated product was purified by recrystallization from ethanol and was identified by melting point (200–201 °C), elemental analysis, and infrared spectra. The molecular weight of the compound is 239.3. The structure of the molecule is given below.

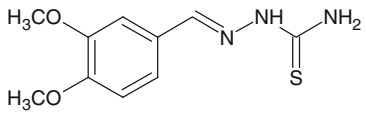

3, 4 dimethoxybenzaldehyde thiosemicarbazone

2.2 Medium

Standard solution of 0.5 M sulfuric acid was prepared by diluting analar grade 98% sulfuric acid by using double distilled water. The solutions of inhibitor with 1×10^{-4}, 2×10^{-4}, 4×10^{-4}, 6×10^{-4} and 8×10^{-4} M concentration were prepared in 0.5 M sulfuric acid. Experiments were carried out using calibrated thermostat at temperatures 30 °C, 35 °C, 40 °C, 45 °C,and 50 °C (± 0.5 °C).

2.3 Electrochemical measurement

Electrochemical measurements were carried out using an electrochemical work station Auto Lab 30, GPES, and FRA software. Both polarization studies and EIS measurements were carried out using conventional three-electrode Pyrex glass cell with platinum counter electrode and saturated calomel electrode (SCE) as reference electrode. All the values of potential are referred to the SCE. The polarization studies were done immediately after the EIS studies on the same electrode without any further surface treatment.

2.3.1 Tafel polarization studies

Finely polished maraging steel specimens were exposed to corrosion medium of sulfuric acid in the presence and

absence of inhibitor at different temperatures (30–50 °C) and allowed to establish a steady-state open circuit potential(OCP). The potentiodynamic current–potential curves were recorded by polarizing the specimen to −250 mV cathodically and +250 mV anodically with respect to OCP at a scan rate of 1 mV s^{-1}.

2.3.2 *Electrochemical impedance spectroscopy (EIS) studies*

In EIS technique, a small amplitude ac signal of 10 mV and frequency spectrum from 100 kHz to 0.01 Hz was impressed at the OCP, and impedance data were analyzed using Nyquist plots. The charge transfer resistance, R_{ct} was extracted from the diameter of the semicircle in Nyquist plot.

In all the above measurements, at least three similar results were considered, and their average values are reported.

2.4 Scanning electron microscope studies (SEM)

The SEM images were recorded using JEOL JSM-6380LA analytical scanning electron microscope.

3 Results and discussion

3.1 Tafel polarization measurement

The corrosion inhibition of aged maraging steel was investigated in 0.5 M sulfuric acid containing various concentrations of DMBTSC inhibitor at different temperatures using Tafel polarization technique. Figure 1 represents Tafel polarization curves of the specimen in 0.5 M sulfuric acid containing different concentrations of inhibitor under study at 30 °C. The percentage inhibition efficiency (IE %) was calculated from expression (1):

$$\mathrm{IE}\% = \frac{I_{\mathrm{corr}} - I_{\mathrm{corr(inh)}}}{I_{\mathrm{corr}}} \times 100 \qquad (1)$$

where I_{corr} and $I_{\mathrm{corr(inh)}}$ are the corrosion current densities in the absence and in the presence of inhibitor, respectively. The corrosion rate is calculated using Eq. 2:

$$\text{Corrosion rate } \left(\mathrm{mm\ y^{-1}}\right) = \frac{3270 \times M \times I_{\mathrm{corr}}}{\rho \times Z} \qquad (2)$$

where 3270 is a constant that defines the unit of corrosion rate, I_{corr} = corrosion current density in A $\mathrm{cm^{-2}}$, ρ = density of the corroding material, 8.23 g $\mathrm{cm^{-3}}$, M = Atomic mass of the metal, and Z = Number of electrons transferred per metal atom [21].

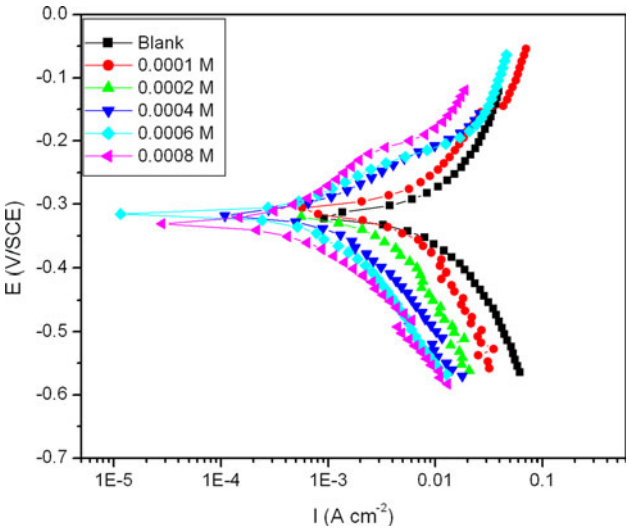

Fig. 1 Tafel polarization curves for the aged maraging steel in 0.5 M sulfuric acid containing different concentrations of inhibitor

The valuable potentiodynamic polarization parameters including corrosion potential (E_{corr}), corrosion current (I_{corr}), corrosion rate (CR), anodic and cathodic slopes (b_a and b_c), and inhibition efficiency (%IE) were calculated from Tafel plots and are summarized in Table 2. The polarization resistance (R_p) increased with increase in inhibitor concentration, suggesting a hindrance to charge transfer reaction (metal dissolution). The value of I_{corr} decreases with increase in the concentration of inhibitor.

As can be seen from the data, addition of DMBTSC decreases the corrosion of the annealed maraging steel sample. Inhibition efficiency increases with increasing DMBTSC concentration. The changes in both the anodic and cathodic Tafel slopes observed on the addition of DMBTSC indicate that both anodic and cathodic reactions are affected by the addition of inhibitor. The addition of DMBTSC affects anodic dissolution of metal and also the hydrogen evolution reaction at the cathode.

No definite trend is observed in the shift of E_{corr} values, which suggests that DMBTSC acts as a mixed type inhibitor [22]. According to Ferreira et al and Li et al.[23, 24], if the displacement in corrosion potential is more than ±85 mV with respect to corrosion potential of the blank, then the inhibitor can be considered as a cathodic or anodic type. However, the maximum displacement in this study is 10 mV, which indicates that DMBTSC is a mixed type inhibitor.

The parallel cathodic Tafel curves suggest that the hydrogen evolution is activation controlled, and the reduction mechanism is not affected by the presence of the inhibitors [22]. The values of b_c changes with increase in inhibitor concentration which indicates the influence of DMBTSC on the kinetics of hydrogen evolution. The shift in the anodic Tafel slope b_a may be due to the sulfate/inhibitor molecules adsorbed on the steel surface [25].

Table 2 Results of Tafel polarization studies on aged maraging steel in 0.5 M sulfuric acid containing different concentrations of DMBTSC

Temp. (°C)	Conc. of inhibitor ($\times 10^{-4}$ M)	E_{corr} (V/SCE)	$-b_c$ (V dec^{-1})	b_a (V dec^{-1})	I_{corr} (mA cm^{-2})	C.R (mm y^{-1})	IE%
30	0	−0.318	0.107	0.103	7.52	87.23	
	1	−0.317	0.120	0.075	3.34	38.74	48.2
	2	−0.318	0.133	0.097	2.26	26.22	64.9
	4	−0.309	0.112	0.113	0.97	11.25	84.8
	6	−0.311	0.113	0.124	0.71	8.24	89.0
	8	−0.310	0.112	0.083	0.64	7.42	91.5
35	0	−0.312	0.122	0.127	8.39	97.32	
	1	−0.314	0.118	0.080	4.45	51.62	43.0
	2	−0.315	0.122	0.078	2.62	30.39	63.4
	4	−0.308	0.106	0.085	1.53	17.75	81.9
	6	−0.310	0.112	0.081	1.13	13.11	85.8
	8	−0.311	0.072	0.088	0.54	6.26	90.1
40	0	−0.309	0.112	0.127	9.65	111.94	
	1	−0.312	0.109	0.108	5.04	58.46	39.0
	2	−0.311	0.157	0.112	3.05	35.38	63.2
	4	−0.307	0.123	0.124	1.75	20.30	78.8
	6	−0.309	0.119	0.119	1.39	16.12	83.0
	8	−0.313	0.102	0.110	1.03	11.95	89.4
45	0	−0.312	0.118	0.118	10.75	124.70	
	1	−0.308	0.125	0.121	7.03	81.55	29.8
	2	−0.310	0.100	0.102	3.78	43.85	57.1
	4	−0.308	0.118	0.082	2.79	32.36	69.2
	6	−0.308	0.109	0.088	1.62	18.79	81.6
	8	−0.312	0.125	0.116	1.24	14.38	88.4
50	0	−0.311	0.112	0.110	11.72	135.95	
	1	−0.302	0.099	0.089	7.50	87.00	25.4
	2	−0.308	0.118	0.088	4.69	54.40	53.2
	4	−0.305	0.114	0.124	3.86	44.78	61.7
	6	−0.307	0.117	0.138	1.88	21.81	81.2
	8	−0.309	0.124	0.116	1.56	18.10	84.7

For anodic polarization curves of specimen with 0.0006 M and 0.0008 M DMBTSC (in Fig. 1), it seems that at the working electrode potential, higher than −200 mV/SCE, the presence of inhibitor does not change the current versus potential characteristics. This potential can be defined as desorption potential [26]. The phenomenon may be due to the obvious metal dissolution, which leads to desorption of the inhibitor molecule from the electrode surface. In this case, the desorption rate of the inhibitor is higher than its adsorption rate, and so the corrosion current increases more obviously with rising potential [27].

3.1.1 *Effect of temperature*

The effect of temperature on the inhibited acid–metal reaction is highly complex because many changes occur on the metal surface, such as rapid etching and desorption of the inhibitor and the inhibitor itself, which in some cases may undergo decomposition and/or rearrangement [28]. However, it facilitates the calculation of many thermodynamic functions for the inhibition and/or the adsorption processes which contribute to determine the type of adsorption of the studied inhibitors. In this study, with increase in solution temperature, corrosion potential (E_{corr}), anodic Tafel slope (b_a), and cathodic Tafel slope (b_c) values are not affected much. This indicates that increase in temperature does not change the mechanism of corrosion reaction. However, I_{corr} and hence the corrosion rate of the specimen increase with increase in temperature for both blank and inhibited solutions. The inhibition efficiency decreases with increase in temperature which indicates desorption of inhibitor molecules [29]. However, this decrease is small at higher concentration of inhibitor.

The apparent activation energy (E_a) for the corrosion process in the presence and absence of inhibitor can be calculated using Arrhenius law Eq. 3 [30].

$$\ln(\mathrm{CR}) = B - (E_a/RT) \quad (3)$$

where B is a constant which depends on the metal type, and R is the universal gas constant. The plot of ln(corrosion rate) versus reciprocal of absolute temperature $1/T$ gives straight line whose slope $= -E_a/R$ gives activation energy for the corrosion process. The Arrhenius plots for the annealed specimen are shown in Fig. 2.

The entropy and enthalpy of activation values for the dissolution of alloy (ΔH_a & ΔS_a) were calculated from transition state theory Eq. 4 [31].

$$\mathrm{CR} = (RT/Nh)\exp(\Delta S_a/R)\exp(-\Delta H_a/RT) \quad (4)$$

where h is Plank's constant, and N is Avagadro's number. A plot of ln(corrosion rate/T) versus $1/T$ gives straight line with slope $= -\Delta H_a/R$ and intercept $= \ln(R/Nh) + \Delta S_a/R$. The calculated values of ΔH_a and ΔS_a are given in Table 3. The plot of ln(corrosion rate/T) versus $1/T$ for the annealed samples of maraging steel in various concentrations of inhibitor in 0.5 M sulfuric acid is shown in Fig. 3.

The calculated values of activation parameters are given in Table 3.

The effect of chemically stable surface active inhibitors is to increase the energy of activation and to decrease the surface area available for corrosion [32]. The value of activation energy (E_a) in 0.5 M sulfuric acid solution containing inhibitor is greater than that without inhibitor. The extent of increase is proportional to the inhibitor concentration, indicating that the energy barrier for the corrosion reaction increases with increase in DMBTSC concentration. The increase in apparent activation energy

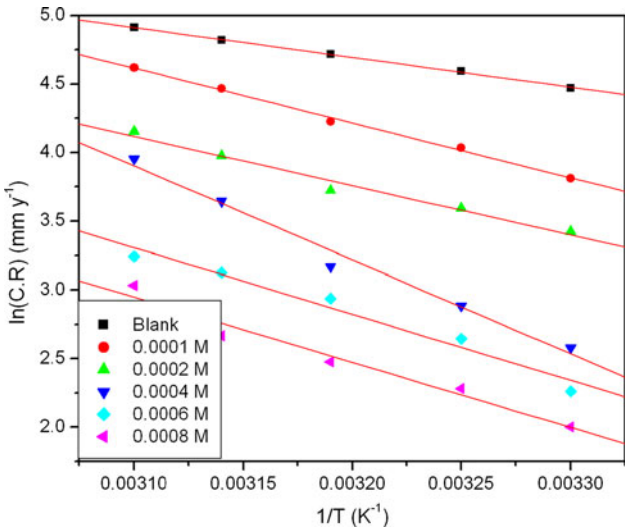

Fig. 2 Arrhenius plots for the dissolution of aged maraging steel in 0.5 M sulfuric acid containing different concentrations of inhibitor

Table 3 Activation parameters for the corrosion of aged maraging steel in 0.5 M sulfuric acid containing different concentrations of inhibitor

Conc. of inhibitor ($\times 10^{-4}$M)	E_a (kJ mol^{-1})	ΔH_a (kJ mol^{-1})	ΔS_a (J mol^{-1} K^{-1})
0	18.1	15.5	−156.7
1	30.0	27.4	−126.3
2	33.4	30.8	−111.8
4	39.9	37.3	−105.5
6	45.2	43.6	−66.8
8	47.4	54.4	−44.6

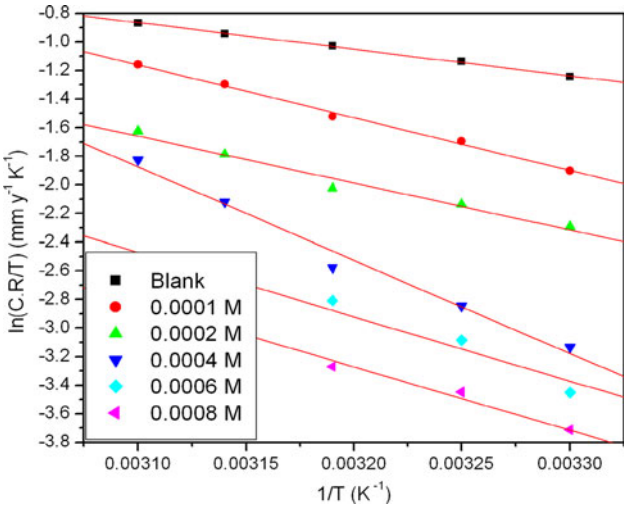

Fig. 3 ln(corrosion rate)/T versus $1/T$ for aged maraging steel in 0.5 M sulfuric acid containing different concentrations of inhibitor

E_a may be interpreted as due to physical adsorption [33] of the inhibitor, which results in increase in surface coverage with the increase in the concentration of the inhibitor. The decrease in the inhibition efficiency of DMBTSC with increase in temperature can be attributed to an appreciable decrease in the adsorption of the inhibitor on the metal surface with increase in temperature and a corresponding increase in corrosion rate because greater area of metal is exposed to the acid [34].

The entropy of activation values in the absence and presence of inhibitor are large and negative. This implies that the activated complex in the rate-determining step represents an association rather than dissociation step, resulting in a decrease in randomness on going from reactants to activated complex [35, 36]. The entropy of activation values are less negative for inhibited solutions than that for the uninhibited solutions. This suggests that an increase in randomness occurred while moving from reactants to the activated complex. This might be the result of the adsorption of organic inhibitor molecules from the

acidic solution, which could be regarded as a quasi-substitution process between the organic compound in the aqueous phase and water molecules at electrode surface [37]. In this situation, the adsorption of organic inhibitor is accompanied by desorption of water molecules from the surface. Thus, the increase in entropy of activation was attributed to the increase in solvent entropy [38].

3.2 Adsorption isotherm

Organic corrosion inhibitors are known to decrease metal dissolution via adsorption on the metal/corrodent interface to form a protective film which separates the metal surface from the corrosive medium. The adsorption route is usually regarded as a substitution process between the organic inhibitor in the aqueous solution [$Inh_{(sol)}$] and water molecules adsorbed at the metal surface [$H_2O_{(ads)}$] as given below[39]:

$$Inh_{(sol)} + \chi H_2O_{(ads)} \leftrightarrow \ Inh_{(ads)} + \chi H_2O_{(sol)} \quad (5)$$

where χ represents the number of water molecules replaced by one molecule of adsorbed inhibitor. The adsorption bond strength is dependent on the composition of the metal, corrodent, inhibitor structure, concentration and orientation as well as temperature. Basic information on the interaction between the inhibitor and alloy surface can be provided by adsorption isotherm. In order to obtain isotherm, the linear relation between surface coverage (θ) value and C_{inh} must be found. Attempts were made to fit the θ values to various isotherms including Langmuir, Temkin, Frumkin, and Flory–Huggins isotherms. By far, the best fit is obtained with the modified Langmuir adsorption isotherm. The following Eq. 6 can be used:

$$\frac{C_{inh}}{\theta} = \frac{1}{K} + C_{inh} \quad (6)$$

where C_{inh} is the concentration of inhibitor, K is the equilibrium constant for adsorption process, and θ is the degree of the surface coverage, which is calculated using Eq. 7.

$$\theta = \frac{IE\%}{100} \quad (7)$$

where IE% is percentage inhibition efficiency as calculated using Eq. 1.

This model has also been used for other inhibitor systems [39–41]. The plot of C_{inh}/θ versus C_{inh} gives a straight line with intercept $1/K$ as shown in Fig. 4.

The values of standard free energy of adsorption are related to K by the relation (8).

$$K = \frac{1}{55.5} e^{\left(-\frac{\Delta G^0_{ads}}{RT}\right)} \quad (8)$$

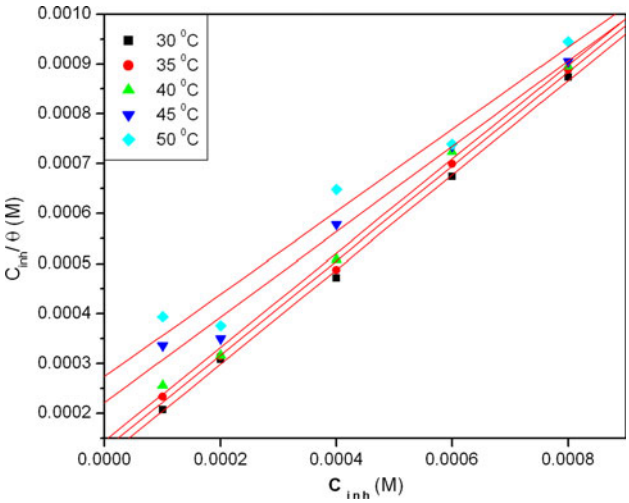

Fig. 4 Langmuir adsorption isotherm of DMBTSC on aged maraging steel in 0.5 M sulfuric acid at different temperatures

where the value 55.5 is the concentration of water in solution in M (mol/L), R is the universal gas constant and T is absolute temperature [42–44]. The thermodynamic data obtained from adsorption isotherm are tabulated in Table 4. The correlation coefficient (R^2) was used to choose the isotherm that best fit the experimental data [28]. The linear regression coefficients are close to unity, and the slopes of straight lines are nearly unity, suggesting that the adsorption of DMBTSC obeys Langmuir's adsorption isotherm, and there is negligible interaction between the adsorbed molecules [24]. The high values of K for the studied inhibitor indicate strong adsorption of inhibitor on the alloy surface. Negative values of ΔG^0_{ads} are the characteristic feature of strong spontaneous adsorption for the studied compounds, which also reflect the high values of inhibition. The negative ΔG^0_{ads} values calculated from Eq. 8 are consistent with the spontaneity of the adsorption process and the stability of the adsorbed layer on the maraging steel surface. In general, the standard free energy values of -20 kJ mol^{-1} or less negative are associated with an electrostatic interaction between charged molecules and charged metal surface, resulting in physisorption, and those of -40 kJ mol^{-1} or more negative involve charge sharing or transfer from the inhibitor molecules to the metal surface to form a coordinate covalent bond, resulting in chemisorption [44–46]. The ΔG^0_{ads} values obtained for the studied inhibitor on the alloy surface in 0.5 M sulfuric acid range from -30 to -32 kJ/mol, indicating both physical and chemical adsorptions [47].

A plot of ΔG^0_{ads} versus T in Fig. 5 was used to calculate the heat of adsorption ΔH^0_{ads} and the standard adsorption entropy ΔS^0_{ads} according to the thermodynamic Eq. 9.

$$\Delta G^0_{ads} = \Delta H^0_{ads} - T\Delta S^0_{ads} \quad (9)$$

Figure 5 clearly shows that the good dependence of ΔG^0_{ads} on T indicates good correlation among thermodynamic parameters. The thermodynamic data obtained for DMBTSC using Langmuir adsorption isotherm are depicted in Table 4.

The values of thermodynamic parameters for the adsorption of inhibitors can provide valuable information about the mechanism of corrosion inhibition. While an endothermic adsorption process ($\Delta H^0_{ads} > 0$) is attributed unequivocally to chemisorption [48], an exothermic adsorption process ($\Delta H^0_{ads} < 0$) may involve either physisorption or chemisorption or a mixture of both the processes. In an exothermic process, physisorption is distinguished from chemisorption by considering the absolute value of adsorption enthalpy. Typically, the enthalpy of a physisorption process is lower than 41.86 kJ mol^{-1}, while that of a chemisorption process approaches 100 kJ mol^{-1} [49]. In the present case, the calculated value of ΔH^0_{ads} is -69.014 kJ mol^{-1}, which is an intermediate case [47], probably involving both physisorption and chemisorption. The ΔS^0_{ads} value is large and negative, indicating that an ordering takes place when the inhibitor gets adsorbed on the metal alloy surface.

3.3 Electrochemical impedance spectroscopy

The results of potentiodynamic polarization experiments were compared with the results of impedance measurements, since EIS is a powerful technique in studying corrosion mechanism. In order to get more information about the corrosion inhibition of aged maraging steel specimens in 0.5 M sulfuric acid containing different concentrations of DMBTSC, EIS measurements were carried out at different temperatures. The Nyquist plots obtained for aged samples of maraging steel specimens in 0.5 M sulfuric acid containing various concentrations of DMBTSC are as shown in Fig. 6.

It is clear from the figures that the shapes of the impedance plots for inhibited specimen are not substantially

Table 4 Thermodynamic parameters for the adsorption of DMBTSC on aged maraging steel surface in 0.5 M sulfuric acid at different temperatures

Temp. (°C)	K ($\times 10^4$) (mol^{-1} L)	$-\Delta G^0_{ads}$ (kJ mol^{-1})	R^2	ΔH^0_{ads} (kJ mol^{-1})	ΔS^0_{ads} (J mol^{-1} K^{-1})
30	0.9070	33.1	0.9993		
35	0.7802	32.7	0.9442	−69.014	−118
40	0.6905	32.4	0.9401		
45	0.4505	31.4	0.9942		
50	0.3647	30.8	0.9818		

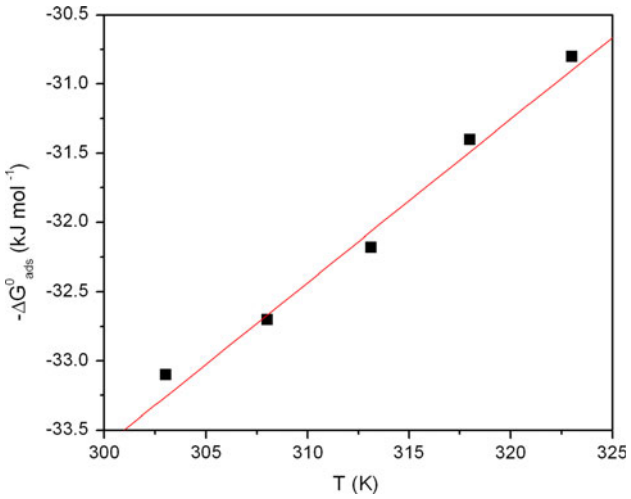

Fig. 5 Plot of ΔG^o_{ads} versus temperature for the adsorption of DMBTSC on aged maraging steel in 0.5 M sulfuric acid

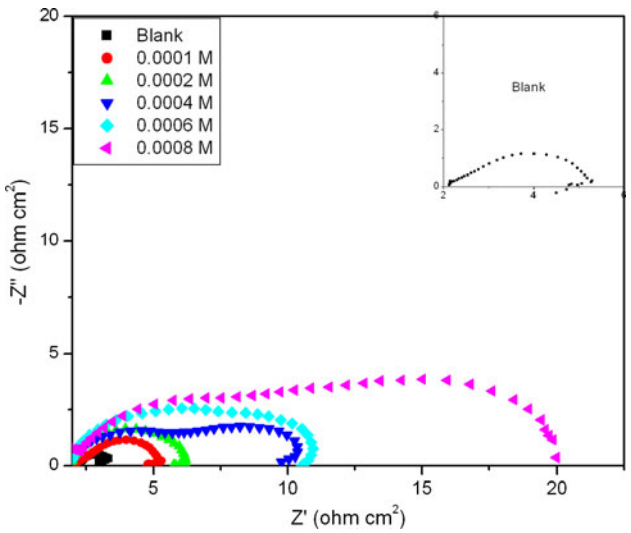

Fig. 6 Nyquist plots for aged maraging steel specimen in 0.5 M sulfuric acid containing different concentrations of inhibitor. Insert blank

different from those of uninhibited one. The presence of inhibitor increases the impedance but does not change other aspects of the behavior. These results support the results of polarization measurements that the inhibitor does not alter the mechanism of electrochemical reactions responsible for corrosion. It inhibits corrosion primarily through its adsorption on the metal surface [50]. The impedance plots are with a depressed capacitive loop at high-frequency range (HF) whose diameter increases with increase in inhibitor concentration, followed by an inductive loop at low-frequency (LF) region. The depressed capacitive loop with its center below the real axis may be due to the contribution from surface roughness, distribution of active

sites, adsorption of inhibitors, and formation of porous layers as reported by others [51]. The HF capacitive loop can be attributed to charge transfer reaction and time constant of the electric double layer [47]. These are not perfect semicircles, because the Nyquist plots obtained in the real system represent a general behavior where the double layer at the metal solution interface does not behave as an ideal capacitor [52, 53]. The LF inductive loop can be attributed to the relaxation process obtained by adsorbed sulfate ions and protons [50, 54]. It may also be attributed to the re-dissolution of the passivated surface at low frequencies [55]. In the present case, the LF inductive loop can be attributed to surface dissolution process. It is also seen from the Fig. 6 that the size of the inductive loop decreases with the increase in inhibitor concentration and almost disappears at the highest concentration of the inhibitor added. The above observations suggest that with the increase in the surface coverage of the alloy as the inhibitor concentration is increased, the rate of alloy dissolution decreases.

The impedance spectra were analyzed by fitting the experimental data to the equivalent circuit model as given in Fig. 7 which has been used previously to model iron/acid interface [50, 56]. In this equivalent circuit, R_S is the solution resistance, and R_{ct} is the charge transfer resistance, R_L and L represent the inductive elements. This also consists of constant phase element, CPE (Q) in parallel to the resistors R_{ct} and $R_{L,}$ which are in series to each other. The CPE is in parallel with the inductor L. The polarization potential, R_P is given by the expression:

$$R_P = R_{ct} + R_L \tag{10}$$

The point of intersection between inductive loop and the real axis represents ($R_s + R_{ct}$). R_s represents the solution resistance due to the ohmic resistances of corrosion product films and the solution enclosed between the working electrode and the reference electrode. R_{ct} represents the charge transfer resistance whose value is a measure of resistance against electron transfer across the surface and is inversely proportional to corrosion rate [57]. The presence of inductor L in the equivalent circuit in the presence of inhibitor indicates that alloy is still dissolved by the direct

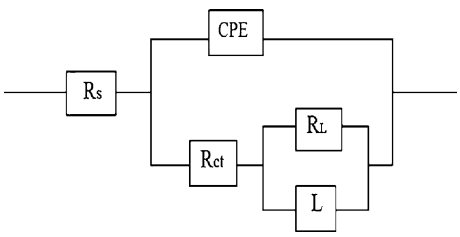

Fig. 7 Equivalent circuit used to fit experimental EIS data for the corrosion of maraging steel specimen in sulfuric acid

charge transfer at the inhibitor-adsorbed alloy surface [58]. The CPE is introduced in the circuit instead of pure double layer capacitor to give more accurate fit [59]. The impedance of CPE is expressed as

$$Z_{CPE} = \frac{1}{Y_0(j\omega)^n} \tag{11}$$

where the amplitude Y_0 and n are frequency independent, and ω is the angular frequency for which $-Z$ reaches its maximum values, n is dependent on the surface morphology: $-1 \leq n \leq 1$. The HF loops have depressed semicircular appearance, with $0.5 \leq n \leq 1$, which is often referred to as frequency dispersion as a result of the non-homogeneity or roughness [54, 60].

The corrosion current density I_{corr} can be calculated using charge transfer resistance R_{ct}, together with Stern–Geary Eq. 11 [57].

$$I_{corr} = \frac{b_a b_c}{2.303 R_{ct} A (b_a + b_c)} \tag{12}$$

The charge transfer resistance R_{ct} and double layer capacitance C_{dl} were determined by the analysis of Nyquist plot and their values are given in Table 5.

The inhibition efficiency in different concentrations of DMBTSC was calculated from the charge transfer resistance according Eq. 13

$$IE\% = \left(\frac{R_{ct} - R_{ct}^0}{R_{ct}}\right) \times 100 \tag{13}$$

where R_{ct} and R_{ct}^0 represent the charge transfer resistance in the presence and absence of inhibitor. The values of R_{ct} increases with increase in the inhibitor concentration, and the results indicate that charge transfer process mainly controls the corrosion process.

The double layer capacitances C_{dl}, for a circuit including CPE were calculated from the following Eq. [61]:

$$C_{dl} = Y_0 (w_{max})^{n-1} \tag{14}$$

where $w_{max} = 2\pi f_{max}$, and f_{max} is the frequency at which the imaginary component of the impedance is maximal. According to the expression of the double layer capacitance presented in the Helmholtz model [25],

$$C_{dl} = \frac{\varepsilon \varepsilon_0}{d} S \tag{15}$$

where d is the thickness of the film, S is the surface area of the electrode, ε_0 is the permittivity of air, and ε is the local dielectric constant.

The value of C_{dl} decreases due to the adsorption of inhibitor molecules, which displaces water molecules originally adsorbed on the mild steel surface and decreases the active surface area. The values of double layer capacitance decreases with increase in inhibitor concentration

Table 5 EIS data of aged maraging steel in 0.5 M sulfuric acid in the absence and presence of different concentrations of inhibitor, DMBTSC

Temp. (°C)	Inhibitor conc. (mol^{-1} dm^3)	R_{ct} (ohm cm^2)	C_{dl} (mF cm^{-2})	IE%
30	0	1.8	29.6	
	1	3.3	10.3	45.0
	2	6.4	9.4	71.9
	4	9.5	8.8	81.1
	6	13.0	4.9	86.6
	8	20.0	2.7	91.1
35	0	1.7	48.0	
	1	2.8	19.2	39.3
	2	5.7	14.4	70.2
	4	7.6	6.7	77.6
	6	10.2	4.8	83.3
	8	18.6	3.4	90.9
40	0	1.6	100.0	
	1	2.6	52.0	38.5
	2	4.5	27.0	64.5
	4	5.7	21.0	71.9
	6	6.8	15.0	76.5
	8	10.4	10.0	85.7
45	0	1.4	430.0	
	1	2.1	340.0	33.6
	2	3.2	215.0	56.3
	4	4.5	111.8	68.8
	6	5.6	77.4	74.9
	8	11	64.2	87.2
50	0	1.2	502.0	
	1	1.5	381.0	20.1
	2	2.2	276.0	45.5
	4	2.8	180.0	57.1
	6	4.9	88.8	75.5
	8	7.2	75.2	83.3

indicating that inhibitor molecules function by adsorption at the metal/solution interface, leading to formation of a protective film on the alloy surface, and decreasing the extent of dissolution reaction [62]. The inhibition efficiency values obtained by the electron impedance method are in good agreement with the ones obtained by Tafel's method.

3.4 Mechanism of corrosion inhibition

Aged maraging steel results from the precipitation of intermetallics. Since these intermetallics have different composition than the bulk metal matrix, their electrochemical behavior is expected to be different from that of the matrix [63]. Also, there will be strain fields around these coherent precipitates as a result of lattice mismatch between the precipitate and the matrix due to the difference in the crystal structure and lattice parameters. These strain fields in combination with the galvanic effect due to the composition difference lead to the enhanced corrosion of aged maraging steel in acid medium. Considering the inhomogeneous nature, the surface of alloy is generally characterized by multiple adsorption sites having different activation energies and heats of adsorption. Inhibitor molecules may thus be adsorbed more readily at surface active sites having suitable adsorption enthalpies.

The adsorption mechanism for a given inhibitor depends on factors, such as the nature of the metal, the corrosive medium, the pH, and the concentration of the inhibitor as well as the functional groups present in its molecule, since different groups are adsorbed to different extents. For instance, S-containing substances have been shown to preferentially chemisorb on the surface of iron in acidic medium, whereas N-containing substances tend to favor physisorption [64]. It is reported that protective value of S-containing compounds is superior to that of N-containing compounds. This may be due to the greater polarizability of the sulphur atom and the presence of two electron pairs available for co-ordination [65].

The inhibition effect of DMBTSC in sulfuric acid solution can be explained as follows: BDTSCO might be protonated in the acid solution as follows:

$$\mathrm{DMBTSC} + x\mathrm{H}^+ \rightarrow [\mathrm{DMBTSCH}_x]^{x+} \quad (16)$$

Thus, in aqueous acidic solution, DMBTSC exists partly in the form of protonated species and partly as neutral molecules. In general, two modes of adsorption could be considered. Taking into consideration of many reported results, Popova et al. [56] concluded that the surface charge of iron in sulfuric acid solution at the free corrosion potential is positive. Therefore, the adsorption of protonated species would be through electrostatic attraction between the positively charged molecule and the negatively charged sulfate ions adsorbed on the metal surface via physisorption. In the study of the effect of inorganic anions and organic compounds on corrosion inhibition of mild steel in various acids, Hackerman et al. [66] have reported that the degree of adsorption of anions was in the order $I^- > Br^- > Cl^- > SO_4^{2-} > ClO^{4-}$. The sulfate ions with low degree of adsorption could not cover the metal surface fully and therefore there is always possibility of the neutral inhibitor molecules occupying the vacant adsorption sites on the metal surface via the chemisorption mode of protection of the corroding surface [67]. The possible bonding sites of the neutral inhibitor are the free electron pairs on sulphur and nitrogen atoms, as well as oxygen, which could interact with vacant *d* orbital of iron [68].

3.5 Scanning electron microscope studies

The SEM images were recorded to establish the interaction of acid medium with the metal surface using JEOL JSM-6380LA analytic scanning electron microscope. The surface morphology of the aged samples was examined by SEM immediately after the sample is subjected to corrosion in H_2SO_4 medium in the absence and in the presence of inhibitor. The SEM image of corroded aged maraging steel sample in Fig. 8 shows degradation of alloy in the absence of inhibitor. The attack by H_2SO_4 is seen to be more at grain boundary since these regions are highly susceptible to corrosion. In aged samples, the intermetallic precipitation at grain boundary may be responsible for the higher rate of corrosion. Figure 9 represents SEM image of aged maraging steel after the corrosion tests in a medium of sulfuric acid containing DMBTSC. The image clearly shows the adsorbed layer of inhibitor molecules on the alloy surface thus protecting the metal from corrosion.

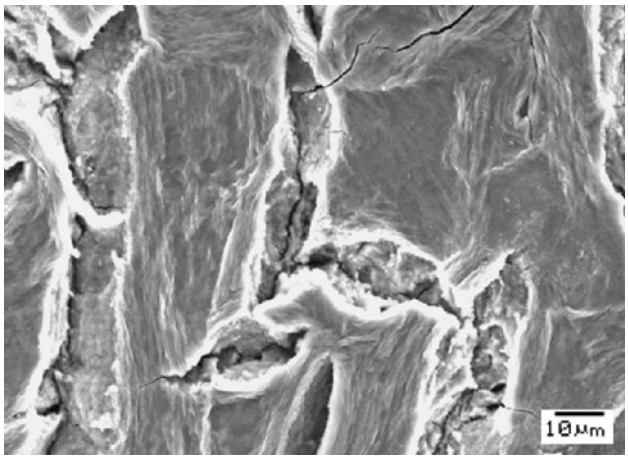

Fig. 8 SEM image of the corroded aged maraging steel after immersion in 0.5 M sulfuric acid

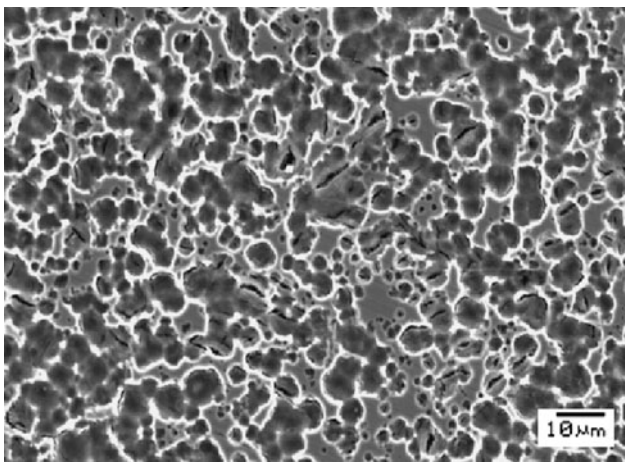

Fig. 9 SEM image of the aged maraging steel after immersion in 0.5 M sulfuric acid containing DMBTSC

4 Conclusions

Potentiodynamic polarization and electrochemical impedance methods were used to evaluate the ability of DMBTSC to inhibit corrosion of aged maraging steel in 0.5 M sulfuric acid. The principal conclusions are

(1) The corrosion of aged maraging steel in 0.5 M sulfuric acid is significantly reduced by the addition of DMBTSC even at low concentration.
(2) The inhibition efficiency increases with increase in inhibitor concentration.
(3) The inhibition efficiency decreases with increase temperature of medium.
(4) DMBTSC acts as mixed type of inhibitor, affecting both anodic and cathodic reactions.
(5) The adsorption of DMBTSC on aged maraging stel surface obeys Langmuir's adsorption isotherm model.
(6) The negative values of ΔG^0_{ads} obtained indicate that DMBTSC adsorbed spontaneously on the aged maraging steel. The adsorption process is exothermic and accompanied by decrease in entropy.
(7) SEM images revealed protection of alloy surface in sulfuric acid medium by the adsorption of DMBTSC.
(8) The inhibition efficiency obtained from potentiodynamic polarization, and EIS techniques are in reasonably good agreement.

References

1. Sastry KY, Narayanan R, Shamantha CR, Sunderason SS, Seshadri SK, Radhakrishnan VM, Iyer KJL, Sundararajan S (2003) Mater Sci Technol 19:375
2. Kurt R, Michael S (1990) ASM handbook Vol 1, 10th edn. Metal park, USA, p 796
3. Lee DG, Jang KC, Kuk JM, Kim IS (2005) J Mater Process Technol 342:162
4. Krick WW, Covert RA, May TP (1968) Met Eng Quart 8:31
5. Dean SW, Copson HR (1965) Corrosion 21:95
6. Bellanger G, Rameau JJ (1996) J Nucl Mater 228:24
7. Bellanger G (1994) J Nucl Mater 217:187
8. Data bulletin on 18%Ni maraging steel (1964) The International Nickel Company, INC
9. Rezek J, Klein IE, Yhalom J (1997) Corros Sci 39:385
10. Sinha PP (1999) IIM Metal News 2:5
11. Singh S, Athar F, Azam A (2005) Bioorg Med Chem Lett 15:5424
12. Jalilian AR, Rowshanfarzad R, Sabet M, Shafiee A (2006) Appl Radiat Isot 64:337
13. Renata BO, Elaine MSF, Rodrigo PPS, Anderson AA, Antoniana UK, Carlos LZ (2008) Eur J Med Chem 43:1984

14. Sanaa T, Arab (2008) Mater Res Bull 43:510
15. Abd El-Nabey BA, Khamis E, Thompson GE, Dawson JL (1986) Surf Coat Technol 28:83
16. Ebenso EE, Ekpe UJ, Ita BI, Offiong OE, Ibok UJ (1999) Mater Chem Phys 60:79
17. EL Shafei AE, Moussa MNH, El-Far AA (2001) Mater Chem Phys 70:175
18. El-Sayed AE, Fouda Abu, El-Nadar H, Moussa MN (1987) Acta Chim Hung 124:581
19. Fang J, Li JJ (2002) J Mol Struct (Theochem) 593:179
20. Larabi L, Harek Y, Benali O, Ghalem S (2005) Prog Org Coat 54:256
21. Fontana MG (1987) Corrosion Engineering, 3rd edn. McGraw-Hill, Singapore
22. Li WH, He Q, Pei CL, Hou BR (2007) Electrochim Acta 52:6386
23. Ferreira ES, Giancomelli C, Giacomelli FC, Spinelli A (2004) Mater Chem Phys 83:129
24. Li WH, He Q, Pei CL, Hou BR (2008) J Appl Electrochem 38:289
25. McCafferty E, Hackerman N (1972) J Electrochem Soc 119:146
26. Lorenz WJ, Mansfeld F (1981) Corros Sci 21:647
27. Aksut AA, Lorenz WJ, Mansfeld F (1982) Corros Sci 22:611
28. Bentiss F, Lebrini M, Lagrenee M (2005) Corros Sci 47:2915
29. Schorr M, Yahalom J (1972) Corros Sci 12:867
30. Bouklah M, Hammouti B, Aounti A, Benhadda T (2004) Prog Org Coat 49:227
31. Abd Ei-Rehim SS, Ibrahim MAM, Khaled KF (1999) J Appl Electrochem 29:595
32. Antropov LI (1967) Corros Sci 7:607
33. El Sherbini EF (1999) Mater Chem Phys 60:286
34. Szauer T, Brand A (1981) Electrochim Acta 26:1219
35. Gomma MK, Wahdan MH (1995) Mater Chem Phys 39:209
36. Marsh J (1988) Advanced organic chemistry, 3rd edn. Wiley Eastern, New Delhi
37. Sahin M, Bilgic S, Yilmaz H (2002) Appl Surf Sci 195:1–4
38. Ateya B, El-Anadouli BE, El-Nizamy FM (1984) Corros Sci 24:509
39. Oguzie EE, Njoku VO, Enenebeaku CK, Akalezi CO, Obi C (2008) Corros Sci 50:3481
40. Sanaa Arab T (2008) Mater Res Bull 43:516
41. Machnikova E, Kenton H, Hackerman N, Whitmire (2008) Electrochim Acta 53:6028
42. Olivares O, Likhanova NV, Gomez B, Navarrete J, Llanos-Serrano ME, Arce E, Hallen JM (2006) Appl Surf Sci 252:2894
43. Kliskic M, Radosevic J, Gudic S, Katalinic V (2000) J Appl Electrochem 30:823
44. Fuchs-Godec R (2006) Colloids Surf A 280:130
45. Hosseini M, Mertens SFL, Arshadi MR (2003) Corros Sci 45:1473
46. Ehteshamzadeh M, Shahrabi T, Hosseini M (2006) Anti Corros Methods Mater 53:296
47. Singh AK, Quraishi MA (2010) Corros Sci 52:156
48. Durnie W, Marco RD, Jefferson A, Kinsella B (1999) J Electrochem Soc 146:17
49. Martinez S, Stern I (2002) Appl Surf Sci 199:83
50. Amin MA, Abd El-Rehim SS, El-Sherbini EEF, Bayyomi RS (2007) Electrochim Acta 52:3588
51. Ec Hosary AA, Saleh RM, Shams El Din AM (1972) Corros Sci 12:897
52. Cheng S, Chen S, Liu T, Chang X, Yin Y (2007) Electrochim Acta 52:5936
53. Ozcan M, Dehri I, Erbil M (2004) Appl Surf Sci 236:159
54. Veloz MA, Gonzalez I (2002) Electrochim Acta 48:135
55. Sherif EM, Park SM (2006) Electrochim Acta 51:1313
56. Popova A, Sokolova E, Raicheva S, Christov M (2003) Corros Sci 45:33
57. El-Sayed A (1997) J Appl Electrochem 27:194
58. Lee WJ (2003) Mater.Sci.Eng A 348:217
59. Boukamamp BA (1980) Solid State Ionics 20:31
60. Hassan HH, Abdelghani E, Amin MA (2007) Electrochim Acta 52:6362
61. Hsu CH, Mansfeld F (2001) Corrosion 57:747
62. Bentiss F, Traisnel M, Lagrenee M (2000) Corros Sci 42:127
63. Shoesmith DW (1987) Metals Handbook, 9th edn. 13:18
64. Fragnani A, Trabanelli G (1999) Corrosion 55:653
65. Stanly Jacob K, Geetha P (2010) Corros Sci 52:224
66. Hackerman N, Snavely ES Jr, Payne JS Jr (1966) J Electrochem Soc 113:677
67. Li X, Deng S, Fu H, Mu G (2009) Corros Sci 51:620
68. Satpati AK, Ravindran PV (2008) Mater Chem Phy 109:352